IEEE Access
Multidisciplinary | Rapid Review | Open Access Journal

Received 29 September 2022, accepted 7 November 2022, date of publication 10 November 2022,
date of current version 28 November 2022.

Digital Object Identifier 10.1109/ACCESS.2022.3221524

RESEARCH ARTICLE

Global Asymptotic Convergent Observer for SLAM

SEYED HAMED HASHEMI AND JOUNI MATTILA
Faculty of Engineering and Natural Sciences, Unit of Automation Technology and Mechanical Engineering, Tampere University, 33100 Tampere, Finland
Corresponding author: Jouni Mattila (jouni.mattila@tuni.fi)

This work was supported by the Academy of Finland under the Project "High Precision Autonomous Mobile Manipulators for Future Digitalized Construction Site" under Grant 335569.

ABSTRACT This paper investigates the global convergence problem of SLAM algorithms, a problem that has been subject to topological obstacles. This is due to the fact that state-space of attitude kinematics, $SO(3)$, is a non-contractible manifold. Hence, $SO(3)$ is not diffeomorphic to Euclidean space. Therefore, existing SLAM algorithms can only guarantee almost global convergence. In order to overcome topological obstructions, this paper introduces a gradient-based hybrid observer that ensures global asymptotic convergence of estimation errors to zero. Moreover, integral action is augmented into the proposed observer to estimate unknown constant bias. Accordingly, a projection scheme is designed to cope with the integral action. Lyapunov stability theorem is used to prove the global asymptotic convergence of the proposed algorithm. Experimental and simulation results are provided to evaluate the performance and demonstrate the effectiveness and robustness of the proposed observer.

INDEX TERMS Geometric observers, global convergence, hybrid systems, simultaneous localization and mapping (SLAM).

I. INTRODUCTION

A. MOTIVATION AND PROBLEM STATEMENT

Simultaneous localization and mapping (SLAM) is a well-known highly nonlinear problem that many previous studies have examined [1]. This estimation problem has an extensive variety of applications, ranging from unmanned aerial vehicles (UAV) to underwater robotics. Likewise, the codependence of environmental mapping and pose estimation makes the problem of significant theoretical interest. In the SLAM problem, an unmanned vehicle tries to construct a map of an environment while simultaneously estimating its pose (i.e., attitude and position) [2]. Different types of estimation techniques have been applied to the SLAM problem, including Kalman-type filters [3], geometric nonlinear observers [4], and optimization-based algorithms [5].

B. LITERATURE REVIEW

As mentioned, the Kalman filter and its variants are estimation algorithms that have most frequently been employed to solve the SLAM problem [6]. Nevertheless, Kalman-type filters suffer from serious shortcomings, such as dependency on the prior information regarding noise statistics and initial values and inconsistency [7]. Several previous studies have addressed these limitations [8]. For instance, [9] introduced a new unscented Kalman-type filter (UKF), called the Adaptive Transformed Unscented Simplex Cubature Kalman Filter, to address the dependency of performance on the initialization and inconsistency problem, which are two key restrictions of UKF. A right invariant extended Kalman filter (RI-EKF) based on a new Lie group structure has also been presented in [10] to address this inconsistency issue. The Masreliez–Martin UKF (MMUKF) has been presented in [11] to overcome problems related to stability and tracking accuracy. In this strategy, an adaptive factor was included to calculate the process noise covariance matrix, and a dynamic robot model was utilized to predict locations of the robot and landmarks. The inconsistency of EKF-SLAM has also been investigated in [12], where filter Jacobians were determined utilizing the first-ever accessible estimates for each state to preserve the dimensions of the observable subspace.

The associate editor coordinating the review of this manuscript and approving it for publication was Ehsan Asadi.

Reference [13] used a combination of EKF and particle filter to address the SLAM problem. In this method, the particle filter determines the position of a mobile robot, and the EKF estimates the position of the environment. The performance of UKF-SLAM was further developed by [14], who rendered an adaptive random search maximization scheme to adapt scaling parameters. To further improve the performance of the standard UKF-SLAM and reduce its dependency on prior knowledge, a robust SLAM has also been developed based on H_∞ square root UKF in [15].

One recently adopted technique for solving the SLAM problem is the use of geometric nonlinear observers. In these techniques, observers are directly designed in matrix Lie groups, including $SE_{1+n}(3)$ and $SLAM_n(3)$. For instance, in [16], a gradient-based observer was designed in the underlying Lie group, where the innovation term was derived from the descent direction of an error function. Utilizing group speed and landmark measurements, [17] introduced a geometric nonlinear observer that evolved directly from the matrix Lie group $SE_{1+n}(3)$. Furthermore, [18] developed a geometric nonlinear observer directly on the manifold of the Lie group $SLAM_n(3)$. This observer guarantees predefined performance parameters and removes unspecified bias in velocity measurements through data obtained from the inertial measurement unit (IMU), group velocity, and landmarks. In a continuation of previous work, the authors have developed the observer by diminishing the boundaries of the error function to ensure faster convergence to the origin [19]. A new SLAM manifold has been introduced in [20] to develop a matrix Lie group $SLAM_n(3)$ for the SLAM problem. Consequently, a global asymptotic stable observer has also been derived on the suggested manifold to solve the SLAM problem in dynamic environments.

Alongside the SLAM problem, Visual SLAM (VSLAM) has also received significant attention. VSLAM is a specific case of SLAM in which a camera provides measurements. Van Goor et al. proposed a new Lie group called $VSLAM_n(3)$ and derived an almost globally asymptotically stable observer on $VSLAM_n(3)$ [21]. The introduced observer utilized decoupled gain matrices for each landmark while employing a new cost function to calculate innovations in robot pose. In addition, [22] continued the authors' prior work, where a gradient-based observer with almost global stability was designed in the $VSLAM_n(3)$ Lie group. The work of Van Goor et al. [21] has been further developed in [23] with the introduction of equivariant group actions. Almost semiglobal convergence is the most important feature of the suggested nonlinear equivariant observer. It is worth noting that optimization-based SLAM techniques are other common approaches for solving VSLAM. For instance, ORB-SLAM is one of the more popular optimization-based algorithms that has received considerable attention [24].

Although the observers described above have a number of advantages, they also share a significant shortcoming. To the best of the authors' knowledge, state-of-the-art observers ensure almost global stability [25] because the special orthogonal group of order three $SO(3)$ is a non-contractible manifold [26]. Hence, there exist sets with Lebesgue measure zero from which the estimation error cannot converge to zero. Therefore, hybrid systems have been used to overcome this topological obstruction and to derive observers with global stability on $SO(3)$ [27], $SE(3)$ [28], and $SE_2(3)$ [29]. For example, two hybrid observers were introduced in [30], where the first observer uses fixed gains, while the second uses variable gains by solving a continuous Riccati equation. Wang et al. [31] expanded on the authors' previous work, with the same strategy being used to develop two hybrid observers. In contrast to previous observers, these observers do not need information about the gravity vector and can overcome difficulties in estimation under intermittent landmark measurements.

C. CONTRIBUTIONS

In light of the shortcomings regarding state-of-the-art solutions, the present paper aims to address the open problem of designing a SLAM observer with global convergence. According to the above discussion, existing approaches for the SLAM problem cannot guarantee global convergence because of the non-contractibility of $SO(3)$ and the existence of Lebesgue measure zero sets. Therefore, the present paper makes use of a hybrid technique to overcome these topological obstacles. Furthermore, an integrator is included in the proposed observer to compensate for unknown bias, leading to an increase in the estimation error. Consequently, the present paper introduces a projection scheme to address the problem associated with the integral action. Hence, the main contributions of the current paper are summarized below.

- A gradient-based hybrid observer is introduced on the $SLAM_n(3)$ manifold, which overcomes topological obstructions and guarantees global asymptotic convergence.
- A Frobenius-norm-based projection scheme is defined to address the integral action. This projection technique preserves bias estimation with known upperbounds and prevents divergence.

D. PAPER ORGANIZATION

The present article is divided into five sections, including the introduction. Section 2 provides the preliminary mathematical notation, SLAM kinematics, and measurements equations, along with a basic background on hybrid systems. The proposed hybrid observer and projection scheme are described in section 3. Section 4 illustrates the experimental and numerical results, where the proposed observer is compared with geometric-type observers and Kalman-type filters. Finally, section 5 summarizes the paper and provides some concluding remarks.

II. PRELIMINARIES

A. NOTATION

The current paper denotes sets of real, non-negative real, and natural numbers by $\mathbb{R}$, $\mathbb{R}_{\geq 0}$, and $\mathbb{N}$, respectively. $\mathbb{R}^n$ represents n-dimensional Euclidean space, where $\{e_i\}_{1\leq i\leq n} \subset \mathbb{R}^n$

is the canonical basis of $\mathbb{R}^n$. $\|x\| = \sqrt{\langle x, x\rangle}$ denotes the two-norm of a vector where $\langle x, y\rangle := x^T y$ is the inner products of vectors $x, y \in \mathbb{R}^n$ and $\|x\|_{\mathcal{A}} := \min_{y\in\mathcal{A}} \|x - y\|$. The trace, determinant, transpose, and skew-symmetric parts of a matrix $A \in \mathbb{R}^{n\times n}$ are denoted by $\mathrm{tr}(A)$, $\det(A)$, A^T, and $\mathrm{skew}(A) = (A - A^T)/2$, respectively. Moreover, $\|A\|_F = \sqrt{\langle A, A\rangle}$ is the Frobenius norm of A, where $\langle A, B\rangle := \mathrm{tr}(A^T B) = (\mathrm{vec}A)^T(\mathrm{vec}B)$, and $\mathrm{vec}A = [Ae_1 \dots Ae_n]^T$ is the vectorization of A. The singular values of A are denoted by σ_i, $i = 1, \dots, n$, where σ_{max} and σ_{min} stand for the maximum and minimum singular values, respectively. The attitude of a rigid body is denoted by $R \in SO(3)$, where $SO(3) := \{R \in \mathbb{R}^{3\times 3} : R^T R = RR^T = I, \det(R) = 1\}$ is the special orthogonal group of order three and $\mathfrak{so}(3) = \{A \in \mathbb{R}^{3\times 3} : A^T = -A\}$ is the Lie algebra of $SO(3)$. In the current paper, $SLAM_n(3) := \{\mathcal{X} = \Psi(R, p, \eta) : R \in SO(3), p \in \mathbb{R}^3, \eta \in \mathbb{R}^{3\times n}\}$ represents the matrix Lie group. Throughout the present paper, the below identities are used frequently.

$$
\begin{aligned}
\Gamma(y) &= \begin{bmatrix} 0 & -y_3 & y_2 \\ y_3 & 0 & -y_1 \\ -y_2 & y_1 & 0 \end{bmatrix}, \\
\varphi(A) &= \frac{1}{2}\begin{bmatrix} A_{(3,2)} - A_{(2,3)} \\ A_{(1,3)} - A_{(3,1)} \\ A_{(2,1)} - A_{(1,2)} \end{bmatrix}, \\
\Psi(R, p, \eta) &= \left[\begin{array}{cc|c} R & p & \eta \\ 0_{1\times 3} & 1 & 0_{1\times n} \\ \hline 0_{n\times 3} & 0_{n\times 1} & I_{n\times n} \end{array}\right], \\
\Upsilon(B) &= \Upsilon\left(\begin{bmatrix} B_1 & B_2 \\ B_3^T & B_4 \end{bmatrix}\right) = \begin{bmatrix} \mathrm{skew}(B_1) & B_2 \\ 0_{n+1\times 3} & 0_{n+1\times n+1} \end{bmatrix}, \\
& y \in \mathbb{R}^3, A, B_1 \in \mathbb{R}^{3\times 3}, B_2, B_3 \in \mathbb{R}^{3\times n+1}, \\
& B_4 \in \mathbb{R}^{n+1\times n+1}
\end{aligned} \tag{1}
$$

The inverse of $\mathcal{X}$ is determined as $\mathcal{X}^{-1} = \Psi(R^T, -R^T p, -R^T\eta)$, and the Lie algebra associated with the $SLAM_n(3)$ is given by

$$
\begin{aligned}
\mathfrak{slam}_n(3) := \{\mathcal{V}(\omega, v, \xi) = &\left[\begin{array}{ccc|c} \Gamma(\omega) & & v & \xi \\ \hline 0_{n+1\times 3} & & 0_{n+1\times 1} & 0_{n+1\times n} \end{array}\right] \\
&: \omega, v \in \mathbb{R}^3, \xi \in \mathbb{R}^{3\times n}\}.
\end{aligned}
$$

The gradient of a differentiable smooth function $m : SLAM_n(3) \to \mathbb{R}$ is denoted by $\nabla_{\mathcal{X}} m \in T_{\mathcal{X}} SLAM_n(3)$, where $T_{\mathcal{X}} SLAM_n(3) := \{\mathcal{X}\mathcal{V} : \mathcal{X} \in SLAM_n(3) \text{ and } \mathcal{V} \in \mathfrak{slam}_n(3)\}$ is the tangent space of $SLAM_n(3)$. Accordingly, $\nabla_{\mathcal{X}} m$ is calculated using the following equation:

$$
dm.\mathcal{X}\mathcal{V} = \langle \nabla_{\mathcal{X}} m, \mathcal{X}\mathcal{V}\rangle_{\mathcal{X}} = \left\langle \mathcal{X}^{-1}\nabla_{\mathcal{X}} m, \mathcal{V}\right\rangle, \tag{2}
$$

where dm is the differential of m and $\langle ., .\rangle_{\mathcal{X}}$ is a Riemannian metric on $SLAM_n(3)$ such that

$$
\langle \mathcal{X}\mathcal{V}_1, \mathcal{X}\mathcal{V}_2\rangle_{\mathcal{X}} = \langle \mathcal{V}_1, \mathcal{V}_2\rangle .
$$

The adjoint map $Ad_{\mathcal{X}} : SLAM_n(3) \times \mathfrak{slam}_n(3) \to \mathfrak{slam}_n(3)$ is defined as $Ad_{\mathcal{X}}\mathcal{V} := \mathcal{X}\mathcal{V}\mathcal{X}^{-1}$. This map takes a tangent vector of one element and transforms it into a tangent vector of another element. Rodrigues formula $\Re : \mathbb{R} \times \mathbb{S}^2 \to SO(3)$ parameterizes a rotation matrix $R \in SO(3)$ using a specific angle $\theta \in \mathbb{R}$ around a fixed axis $y \in \mathbb{S}^2$, which is expressed as follows:

$$
\Re(\theta, y) = I + \sin(\theta)\Gamma(y) + (1 - \cos(\theta))\Gamma^2(y) = \exp(\theta\Gamma(y)), \tag{3}
$$

where $\mathbb{S}^2 := \{y \in \mathbb{R}^3 : \|y\| = 1\}$ is a unit two-dimensional sphere.

B. SLAM KINEMATICS

Kinematic equations that define the motion of a rigid body and family of n landmarks are given as follows:

$$
\dot{R} = R\Gamma(\omega) \tag{4}
$$

$$
\dot{p} = Rv \tag{5}
$$

$$
\dot{\eta}_i = R\xi_i, \quad i = 1, \dots, n \tag{6}
$$

where $\omega \in \mathbb{R}^3$ and $v \in \mathbb{R}^3$ are the angular rate and linear velocity of rigid body expressed in the body-fixed frame $\mathcal{B}$, respectively. $\xi_i \in \mathbb{R}^3$ is the linear speed of i-th landmark expressed in $\mathcal{B}$. Moreover, $p \in \mathbb{R}^3$ and $\eta_i \in \mathbb{R}^3$ denote the position of the rigid body and i-landmarks in the inertial frame $\mathcal{I}$, respectively. The kinematic equations (4)-(6) can be rephrased using the following compact form:

$$
\dot{\mathcal{X}} = \mathcal{X}\mathcal{V}. \tag{7}
$$

In the present paper, it is assumed that landmarks are stationary (i.e., $\xi_i = 0$) and that the linear and angular velocities of the rigid body are available for measurement. It is also assumed that angular and linear velocity measurements include an unknown constant bias, as follows:

$$
\begin{aligned}
&\mathcal{V}_m = \mathcal{V} + \mathcal{V}_b, \\
&\mathcal{V}_m = \mathcal{V}(\omega_m, v_m, 0),\ \mathcal{V}_b = \mathcal{V}(b_\omega, b_v, 0),\ b = [b_\omega\ b_v]^T.
\end{aligned} \tag{8}
$$

It is also assumed that the robot can perceive both range $\theta_b = \|\eta_i - p\|$ and bearing $\jmath = R^T(\eta_i - p)/\theta_b$ relative to landmarks. Accordingly, the following compact equation is the result of a combination of the range and bearing measurements:

$$
\begin{aligned}
\beta_i := \mathcal{X}^{-1} r_i &= \begin{bmatrix} R^T(\eta_i - p) \\ 1 \\ -e_i \end{bmatrix}, \quad i = 1, \dots, n \\
r_i &= \begin{bmatrix} 0_{3\times 1} \\ 1 \\ -e_i \end{bmatrix}
\end{aligned} \tag{9}
$$

C. HYBRID SYSTEM FRAMEWORKS

The present paper uses the following framework of hybrid systems $\mathcal{H}$ first introduced by [32].

$$
\mathcal{H} : \begin{cases} \dot{x} = f(x, u), & (x, u) \in C \\ x^+ = g(x, u), & (x, u) \in D \end{cases} \tag{10}
$$

In this framework, $f : \mathbb{R}^n \times \mathbb{R}^m \to \mathbb{R}^n$ is the flow map that defines the continuous dynamics of $\mathcal{H}$, and $g : \mathbb{R}^n \times \mathbb{R}^m \to \mathbb{R}^n$ is the jump map that specifies the behavior of $\mathcal{H}$ during jumps. The flow set $C \subset \mathbb{R}^n \times \mathbb{R}^m$ indicates where a continuous evolution is allowed to flow, and the jump set $D \subset \mathbb{R}^n \times \mathbb{R}^m$ demonstrates where the system is permitted to jump. Subset $E \subset \mathbb{R}_{\geq 0} \times \mathbb{N}$ is called a hybrid time domain if $E = \bigcup_{i=1}^{I} ([t_i, t_{i+1}], i)$ for finite sequences of times $0 = t_0 \leq t_1 \cdots \leq t_{I+1}$. A hybrid arc consists of a hybrid time domain dom x and a function $x : \text{dom } x \to \mathbb{R}^n$, which is also called a solution to $\mathcal{H}$.

Lemma 1 [33]: The closed set $\mathcal{A} \subset \mathbb{R}^n$ is locally and exponentially stable for $\mathcal{H}$ if $(\alpha_1 > \alpha_2, s_1, s_2, n) \in \mathbb{R}_{\geq 0}$ exist and there is a continuously differentiable function $V : \text{dom } V \to \mathbb{R}$ on an open set containing the closure of C that satisfies the following equation:

$$\begin{aligned} \alpha_2 \|x\|_{\mathcal{A}}^n \leq V(x) \leq \alpha_1 \|x\|_{\mathcal{A}}^n, \\ \forall x \in (C \cup D \cup g(D)) \cap (\mathcal{A} + s_1 \mathbb{B}) \\ \langle \nabla V(x), f \rangle \leq -s_2 V(x), \quad \forall x \in C \cap (\mathcal{A} + s_1 \mathbb{B}) \\ V(g) \leq \exp(-s_2) V(x), \quad \forall x \in D \cap (\mathcal{A} + s_1 \mathbb{B}). \end{aligned} \tag{11}$$

where $\mathbb{B} := \{x \in \mathbb{R}^n : \|x\| \leq 1\}$ is the closed unit ball. The set $\mathcal{A}$ is said to be globally exponentially stable if $s_1 = \infty$, and $\mathcal{A}$ is said to be globally asymptotically stable if $s_1 = \infty$, $s_2 = 0$.

III. PROPOSED OBSERVER AND PROJECTION ALGORITHMS

This section describes the proposed observer and projection method. As mentioned above, the two main techniques that have been utilized to solve the SLAM problem are geometric nonlinear observers and Kalman-type filters. The drawbacks of these methods have also been discussed. Consequently, the current paper has designed a hybrid observer to overcome these drawbacks. Moreover, the integral action is considered in the proposed observer algorithm to estimate constant bias, which leads to an increase in bias estimation. Therefore, a new projection scheme has been designed to address this problem.

A. PROPOSED HYBRID OBSERVER

State-of-the-art observers are almost globally stable because of the non-contractibility of the state-space of attitude kinematics (i.e., $SO(3)$). Consequently, hybrid systems have been used to tackle this topological obstruction and obtain globally stable results [34]. Therefore, the present paper builds on the observer developed by [17], describing a hybrid observer for solving the SLAM problem. Consider the following smooth real-value function: $\mathcal{U} : SLAM_n(3) \to \mathbb{R}$

$$\mathcal{U}(\mathcal{X}) = \frac{1}{2} \text{tr}((I - \mathcal{X}) A (I - \mathcal{X})^T), \tag{12}$$

where $A := \sum_{i=1}^{n} k_i r_i r_i^T$ and $k_i \in \mathbb{R}_{\geq 0}$ are positive constants. Utilizing the Riemannian metric on $SLAM_n(3)$ and the identities provided in the Appendix, one can show the following:

$$\begin{aligned} d\mathcal{U}.\mathcal{X}\mathcal{V} &= \left\langle \mathcal{X}^{-1} \nabla_{\mathcal{X}} \mathcal{U}, \mathcal{V} \right\rangle \Rightarrow \\ d\mathcal{U}.\mathcal{X}\mathcal{V} &= \text{tr}(-A(I - \mathcal{X})^T \mathcal{X}\mathcal{V}) \\ &= \left\langle \Upsilon(\mathcal{X}^{-1}(\mathcal{X} - I)A), \mathcal{V} \right\rangle \\ &= \left\langle \Upsilon((I - \mathcal{X}^{-1})A), \mathcal{V} \right\rangle. \end{aligned} \tag{13}$$

Therefore, the gradient of $\mathcal{U}$ with respect to $\mathcal{X}$ is calculated with the following equation:

$$\nabla_{\mathcal{X}}(\mathcal{U}) = \mathcal{X} \Upsilon((I - \mathcal{X}^{-1})A). \tag{14}$$

Throughout the current paper, $\hat{\mathcal{X}}$ denotes the estimated value of the state $\mathcal{X}$. Therefore, $\tilde{\mathcal{X}} = \mathcal{X}\hat{\mathcal{X}}^{-1}$ is the estimation error with $\tilde{R} = R\hat{R}^T$, $\tilde{p} = p - \tilde{R}\hat{p}$, and $\tilde{\eta} = \eta - \tilde{R}\hat{\eta}$. Hence, the following identity can be easily calculated using (7) and (1).

$$\begin{aligned} &\Upsilon(\sum_{i=1}^{n} k_i (r_i - \hat{\mathcal{X}}\beta_i) r_i^T) = \Upsilon((I - \tilde{\mathcal{X}}^{-1})A), \ (a) \\ &\sum_{i=1}^{n} k_i \|r_i - \hat{\mathcal{X}}\beta_i\|^2 = \text{tr}((I - \tilde{\mathcal{X}})A(I - \tilde{\mathcal{X}})^T), \ (b) \end{aligned} \tag{15}$$

The dynamics of the proposed hybrid observer is defined as follows:

$$\begin{cases} \dot{\hat{\mathcal{X}}} = \hat{\mathcal{X}}(\mathcal{V}_m - \mathcal{V}_{\hat{b}} - \Delta), \\ \dot{\mathcal{V}}_{\hat{b}} = -\Upsilon(\hat{\mathcal{X}}^T \sum_{i=1}^{n} k_i (r_i - \hat{\mathcal{X}}\beta_i) r_i^T \hat{\mathcal{X}}^{-T}), \quad (\hat{\mathcal{X}}, \hat{b}) \in C \\ \dot{q} = 0, \end{cases}$$

$$\begin{cases} \hat{\mathcal{X}}^+ = \mathcal{X}_q, \\ \mathcal{V}_{\hat{b}}^+ = \text{Proj}(\mathcal{V}_{\hat{b}}), \qquad (\hat{\mathcal{X}}, \hat{b}) \in D \\ q^+ = \arg\min_{q \in \mathcal{Q}} \mathcal{U}(\tilde{\mathcal{X}}_q), \end{cases}$$

$$C := \{(\mathcal{U}(\tilde{\mathcal{X}}) - \min_{\tilde{\mathcal{X}}_q \in \mathcal{Q}} \mathcal{U}(\tilde{\mathcal{X}}_q) \leq \delta) \text{ and } (\|\mathcal{V}_{\hat{b}}\|_F \leq \mathfrak{Z})\},$$

$$D := \{(\mathcal{U}(\tilde{\mathcal{X}}) - \min_{\tilde{\mathcal{X}}_q \in \mathcal{Q}} \mathcal{U}(\tilde{\mathcal{X}}_q) \geq \delta) \text{ or } (\|\mathcal{V}_{\hat{b}}\|_F > \mathfrak{Z})\},$$

$$\mathcal{X}_q = \Psi(\Re(q\theta, \ell)' \hat{R}, \Re(q\theta, \ell)\hat{p}, q\hat{\eta}), \quad q \in \mathbb{N}$$

$$\Delta = -Ad_{\hat{\mathcal{X}}^{-1}} \Upsilon(\sum_{i=1}^{n} k_i (r_i - \hat{\mathcal{X}}\beta_i) r_i^T) K,$$

$$\hat{b} = [\varphi(\mathcal{V}_{\hat{b}}(1:3, 1:3))\ \mathcal{V}_{\hat{b}}(1:3, 4)]^T. \tag{16}$$

In (16), $\theta, \delta, \mathfrak{Z} \in \mathbb{R}_{>0}$ are arbitrary constants, $\ell \in \mathbb{S}^2$ is an arbitrary fixed vector, $\mathcal{Q} = \{\mathcal{X}_q \in SLAM_n(3) : q \in \mathbb{N}\}$ is a compact set, $K := k_o I_{n \times n}$ with $k_o \in \mathbb{R}_{>0}$ is the observer gain, and $\tilde{\mathcal{X}}_q = \mathcal{X}\mathcal{X}_q^{-1}$.

Theorem: Consider the proposed hybrid observer (16) with any $\theta \in \mathbb{R}_{>0}$ and $\ell \in \mathbb{S}^2$ for the SLAM kinematics (7). The state estimation error $\tilde{\mathcal{X}}$ and bias estimation error $\mathcal{V}_{\tilde{b}} = \mathcal{V}_b - \mathcal{V}_{\hat{b}}$ converge to $I_{n \times n}$ and 0, respectively. Therefore, the following set is globally asymptotically stable:

$$\begin{aligned} \mathcal{A} := \{(\tilde{\mathcal{X}}, \mathcal{V}_{\tilde{b}}) \in SLAM_n(3) \times \mathfrak{slam}_n(3) \\ : \tilde{\mathcal{X}} = I, \mathcal{V}_{\tilde{b}} = 0\}. \end{aligned} \tag{17}$$

Proof: According to **Lemma 1**, **Theorem** is proven in two steps.

Step 1: This step proves the second condition of (11) with $s_2 = 0$. Utilizing the facts $\dot{\hat{\mathcal{X}}}^{-1} = -\hat{\mathcal{X}}^{-1}\dot{\hat{\mathcal{X}}}\hat{\mathcal{X}}^{-1}$ and $\dot{\mathcal{V}} = \dot{\mathcal{V}}_m = 0$, one has the following:

$$\begin{aligned}\dot{\tilde{\mathcal{X}}} &= \tilde{\mathcal{X}}(Ad_{\hat{\mathcal{X}}}(\Delta - \mathcal{V}_{\tilde{b}}))\\ \dot{\mathcal{V}}_{\tilde{b}} &= -\dot{\mathcal{V}}_{\hat{b}}.\end{aligned} \tag{18}$$

Hence, the estimation error dynamics can be calculated using the following equation:

$$\begin{aligned}\dot{\tilde{\mathcal{X}}} &= \tilde{\mathcal{X}}(-\Upsilon((I - \tilde{\mathcal{X}}^{-1})A)K - Ad_{\hat{\mathcal{X}}}\mathcal{V}_{\tilde{b}})\\ \dot{\mathcal{V}}_{\tilde{b}} &= \Upsilon(\hat{\mathcal{X}}^T(I - \tilde{\mathcal{X}}^{-1})A\hat{\mathcal{X}}^{-T}).\end{aligned} \tag{19}$$

The Lyapunov function candidate is defined as follows:

$$V(\tilde{\mathcal{X}}, \mathcal{V}_{\tilde{b}}) = \mathcal{U}(\tilde{\mathcal{X}}) + \frac{1}{2}\left\|\mathcal{V}_{\tilde{b}}\right\|_F^2. \tag{20}$$

Time derivative of V is calculated as follows:

$$\begin{aligned}\dot{V} &= \left\langle \Upsilon((I - \tilde{\mathcal{X}}^{-1})A), (-\Upsilon((I - \tilde{\mathcal{X}}^{-1})A)K - Ad_{\hat{\mathcal{X}}}\mathcal{V}_{\tilde{b}})\right\rangle\\ &\quad + \left\langle \Upsilon(\hat{\mathcal{X}}^T(I - \tilde{\mathcal{X}}^{-1})A\hat{\mathcal{X}}^{-T}), \mathcal{V}_{\tilde{b}}\right\rangle\\ &= -\left\langle \Upsilon((I - \tilde{\mathcal{X}}^{-1})A), \Upsilon((I - \tilde{\mathcal{X}}^{-1})A)K\right\rangle\\ &\quad - \left\langle \hat{\mathcal{X}}^T(I - \tilde{\mathcal{X}}^{-1})A\hat{\mathcal{X}}^{-T}, \mathcal{V}_{\tilde{b}}\right\rangle\\ &\quad + \left\langle \hat{\mathcal{X}}^T(I - \tilde{\mathcal{X}}^{-1})A\hat{\mathcal{X}}^{-T}, \mathcal{V}_{\tilde{b}}\right\rangle\\ &= -k_o\|\Upsilon((I - \tilde{\mathcal{X}}^{-1})A)\|_F^2.\end{aligned} \tag{21}$$

After simplifying (21) and utilizing the Cauchy–Schwarz inequality for matrix [35], the resulting equation is as follows:

$$\dot{V} \leq -k_o\|\Upsilon((I - \tilde{\mathcal{X}}^{-1})A)\|_F^2 \leq 0. \tag{22}$$

Thus, it can be deduced that $\tilde{R}$, $\tilde{p}$, $\tilde{\eta}$ and $\mathcal{V}_{\tilde{b}}$ are globally bounded. This implies that $\ddot{V}$ is also globally bounded. Barbalat's lemma reveals that $\lim_{t\to+\infty}\dot{V} = 0$; therefore, $\tilde{\mathcal{X}} = I$ and $\mathcal{V}_{\tilde{b}} = 0$ (for details, see [17]).

Step 2: In this step, the last condition of (11) is proven. Because the switching variable q generates jumps, it is essential to assay the variation in $V(\tilde{\mathcal{X}}, \mathcal{V}_{\tilde{b}})$ to ensure that the Lyapunov function is reduced across jumps. The variation in V along jumps is given by the following equation:

$$\begin{aligned}&V(\hat{\mathcal{X}}^+, \mathcal{V}_{\hat{b}}^+) - V(\hat{\mathcal{X}}, \mathcal{V}_{\hat{b}})\\ &= (\mathcal{U}(\hat{\mathcal{X}}^+) + \frac{1}{2}\left\|\mathcal{V}_{\hat{b}}^+\right\|_F^2) - (\mathcal{U}(\hat{\mathcal{X}}) + \frac{1}{2}\left\|\mathcal{V}_{\hat{b}}\right\|_F^2)\\ &= (\mathcal{U}(\mathcal{X}_q) - \mathcal{U}(\hat{\mathcal{X}})) + (\left\|\text{Proj}(\mathcal{V}_{\hat{b}})\right\|_F^2 - \left\|\mathcal{V}_{\hat{b}}\right\|_F^2).\end{aligned} \tag{23}$$

From (16), one can obtain the following:

$$\min_{\tilde{\mathcal{X}}_q \in \mathcal{Q}} \mathcal{U}(\tilde{\mathcal{X}}_q) - \mathcal{U}(\tilde{\mathcal{X}}) \leq -\delta. \tag{24}$$

From the fact $\sigma_{max}(\mathcal{V}_{\hat{b}}) \leq \|\mathcal{V}_{\hat{b}}\|_F$, we have $\left\|\text{Proj}(\mathcal{V}_{\hat{b}})\right\|_F^2 \leq \left\|\mathcal{V}_{\hat{b}}\right\|_F^2$, so we have the following:

$$V(\hat{\mathcal{X}}^+, \mathcal{V}_{\hat{b}}^+) - V(\hat{\mathcal{X}}, \mathcal{V}_{\hat{b}}) \leq 0. \tag{25}$$

Finally, it follows from **Lemma 1** that the set $\mathcal{A}$ is globally asymptotically stable. □

The salient features of the proposed observer are 1) its simplicity, 2) global convergence, and 3) low computational cost.

B. PROPOSED PROJECTION SCHEME

Because of the existence of measurement noise in practical applications, the integral action may cause an enhancement in bias estimation [36]. To address this problem, the present paper introduces a new projection mechanism, as follows:

$$\begin{aligned}&A = \sqcup\text{diag}(\sigma_{max}, \ldots, \sigma_{min})\vee^T, \ (a)\\ &\text{Proj}(A)\\ &\quad = \begin{cases} A, & \text{if } \|A\|_F \leq \gamma,\\ \sqcup\text{diag}(\min(\gamma, \sigma_{max}), & \\ \ldots, \min(\gamma, \sigma_{min}))\vee^T, & \text{otherwise}\end{cases}\end{aligned} \tag{26}$$

Equation (26a) is the singular value decomposition of A, in which $\sqcup$, $\vee$ are unitary matrices. The proposed projection scheme upperbounds the Frobenius norm of A by $\gamma \in \mathbb{R}_{>0}$.

Lemma 2: The following properties hold for the proposed projection scheme:

1) $\|\text{Proj}(.)\|_F \leq \gamma$,
2) Proj(.) is locally Lipschitz continuous.

Proof: The proof of property (1) is clear from the fact that $\sigma_{max}(\text{Proj}(.)) = \min(\gamma, \sigma_{max}) \leq \|\text{Proj}(.)\|_F$. To prove the second property, consider two matrices $A, B \in \mathbb{R}^{n\times n}$. It holds that

$$\begin{aligned}&\|\text{Proj}(A) - \text{Proj}(B)\|_F^2\\ &= \text{tr}((\text{Proj}(A) - \text{Proj}(B))(\text{Proj}(A) - \text{Proj}(B))^T)\\ &= \text{tr}(\text{Proj}(A)\text{Proj}(A)^T) - 2\text{tr}(\text{Proj}(A)\text{Proj}(B)^T)\\ &\quad + \text{tr}(\text{Proj}(B)\text{Proj}(B)^T) = \|\text{Proj}(A)\|_F^2 + \|\text{Proj}(B)\|_F^2\\ &\quad - 2\text{tr}(\text{Proj}(A)\text{Proj}(B)^T).\end{aligned} \tag{27}$$

Accordingly, it follows from Von Neumann's trace inequality [37], which is represented in the Appendix , and the fact $\|\text{Proj}(A)\|_F \leq \|A\|_F$, that

$$\|\text{Proj}(A) - \text{Proj}(B)\|_F \leq \|A - B\|_F. \tag{28}$$

Finally, it can be deduced from (28) that the proposed projection scheme is locally Lipschitz continuous. □

IV. EVALUATION STUDIES

This section presents numerical simulations and experimental results to evaluate the performance of the proposed observer. The proposed hybrid observer is contrasted with the geometric observer, smooth observer, Unscented Kalman Filter (UKF), and Right UKF on Lie Groups (Right-UKF-LG), as described in [17], [21], and [38], respectively. Moreover, two different datasets are utilized to show the robustness of the proposed technique and to verify the stability and convergence of the proposed observer. The experiments were conducted on an Intel Core i5-1145G7 CPU · 2.60GHz desktop PC with 16 GB RAM.

A. SIMULATION RESULTS

This section investigates performance of the proposed method by numerical simulation. It is considered that the robot moves in a circular trajectory at a constant altitude, and it is assumed that it can measure range and bearing to four landmarks located at

$$\eta = \begin{bmatrix} 8 & 0 & -8 & 0 \\ 0 & 8 & 0 & -8 \\ 0 & 0 & 0 & 0 \end{bmatrix}.$$

Moreover, range and bearing measurements contain a noise signal consisting of a uniform distribution on the interval [0 0.4] and a Gaussian distribution with zero mean and unit variance. The following constant biases corrupt the angular velocity and linear velocity $b_\omega = [-0.02\ 0.05\ 0.03]^T$, $b_v = [0.2\ 0.05\ 0.1]^T$, respectively. Unbiased measurements of the angular velocity and linear velocity in the body fixed frame are such that $\omega = [0\ 0\ 0.3]^T$ rad/sec and $v = [1\ 0\ 0]^T$ m/sec. The initial position and attitude of robot were set to $p(0) = [0\ 0\ 2]^T$ and $R(0) = \Re(0, e_1)$, respectively. The initial conditions for both observers were set to $\hat{p}(0) = [0\ 0\ 0]^T$, $\hat{R}(0) = \Re(\pi/6, e_1)$, and $\hat{\eta} = 1.5 * \eta$. Figures (1–4) illustrate the results of this experiment. Figure (1) depicts the estimated path of the robot and the observer landmark trajectories, as well as the actual robot path and true landmark positions. The errors associated with the estimates of the robot's position and landmarks' positions are shown in Figure (2). The evolution of the Lyapunov function and error in the estimation of bias are depicted in Figure (3). The attitude tracking errors are illustrated in Figure (4). This figure reveals that the hybrid observer successfully tracked the true attitude compared with the designed observer in [21]. This figure also proves that the proposed observer breaks topological obstructions and produces rotation for reducing the attitude tracking error. Furthermore, these figures demonstrate that the proposed observer has lower estimation errors than the geometric observer and the convergence rate of the proposed observer is faster than that of the geometric observer.

B. EXPERIMENTAL RESULTS

In this section, the performance of the proposed observer is evaluated by utilizing a real-world EuRoc dataset [39]. The EuRoC dataset consists of synchronized 1) 200 Hz IMU measurements, 2) micro aerial vehicle (MAV) ground truth, and 3) 20 Hz stereo images. The EuRoC provides two kinds of datasets, which were recorded in a large machine hall and in the Vicon room. The present paper considers this dataset for the experimental evaluation because of the violent rotation and considerable lighting variation that make the dataset laborious for VSLAM algorithms. Figure (5) depicts the features extracted from sample images in the V2_01_easy datasets.

1) FIRST EXPERIMENT

This experiment aims to prove that applying a hybrid algorithm to the smooth observer [17] leads to a performance

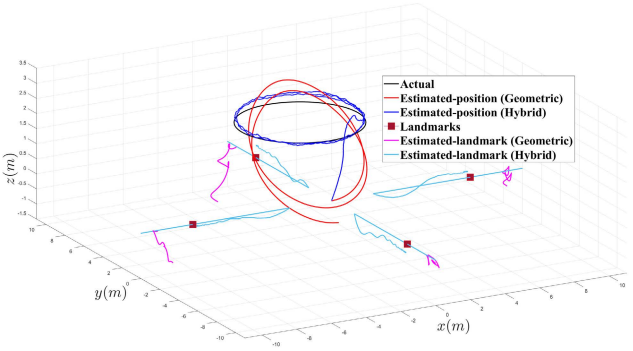

FIGURE 1. 3D trajectories of the observers compared with the actual system evolution.

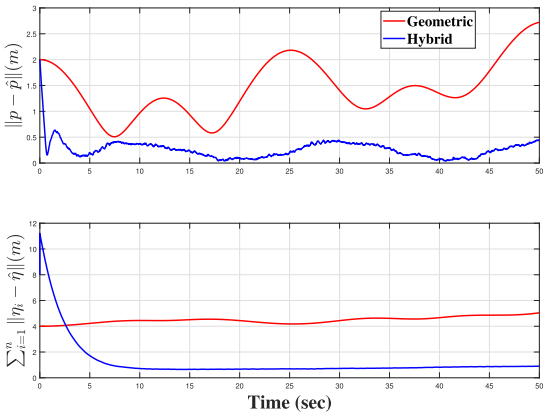

FIGURE 2. Estimation errors of robot position and Landmarks' positions.

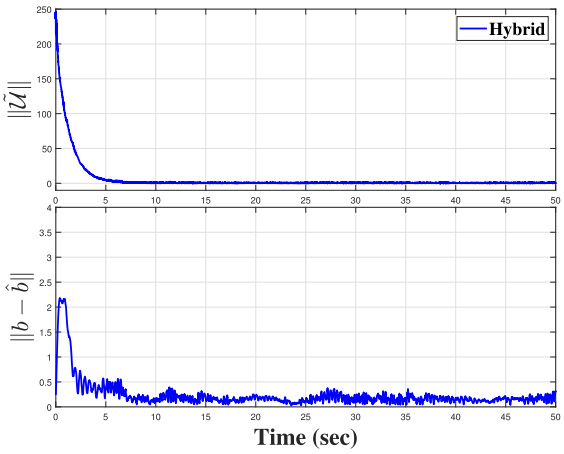

FIGURE 3. Evolution of the Lyapunov function and norm of the velocity bias estimation error versus time.

improvement. In this experiment, the proposed and smooth observers are evaluated on a V2_01_easy of EuRoc public dataset. The estimated trajectories of the observers and their comparisons against the ground truth, which is acquired via a Vicon 6D motion capture system at a rate of 100 Hz, are demonstrated in Figure (6). Here, the observer-estimated trajectory has been aligned to the ground truth by utilizing the

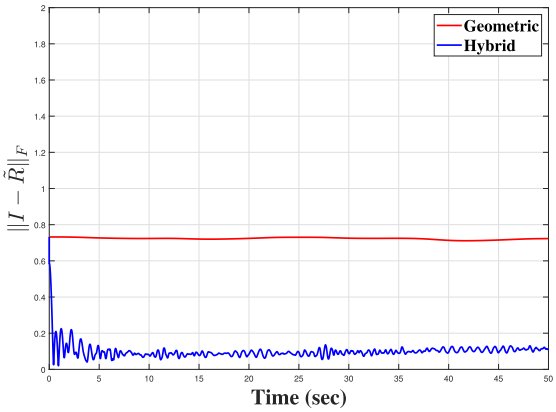

FIGURE 4. Rotation estimation errors versus time.

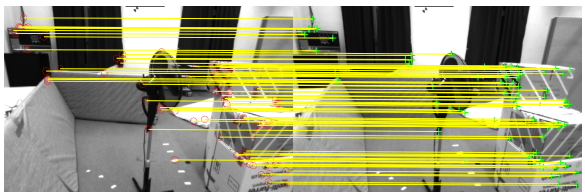

FIGURE 5. Examples of feature tracks between two consecutive keyframes.

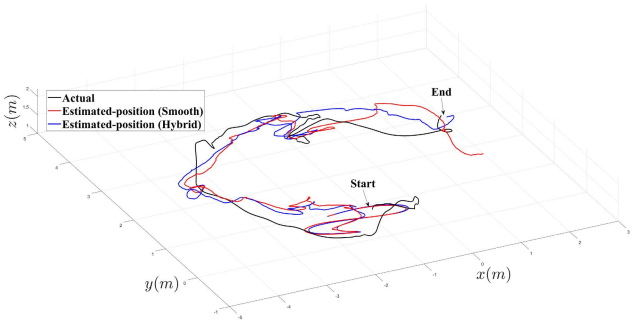

FIGURE 6. Comparison of global trajectories estimated by proposed observer and smooth observer on V2_01_easy sequence.

Umeyama technique [40]. Figure (7) illustrates the position states (x, y, and z) of the observers and ground truth. It can be deduced from these figures that the proposed observer successfully tracked the actual trajectory and finally converged to the true values within an acceptable range of error.

2) SECOND EXPERIMENT

In this experiment, the performance of the hybrid observer is compared with the results acquired utilizing the traditional UKF and Right UKF on Lie Groups (Right-UKF-LG). This experiment tests the performance of proposed method with real-world measurements from the V1_02_medium of EuRoc public dataset. Figure (8) illustrates the estimated trajectories by hybrid observer, UKF, and Right-UKF-LG compared with the ground truth. The true position of MAV and estimated positions in the x, y, z direction are depicted in Figure (9). It is worth noting that UKF and Right-UKF-LG are

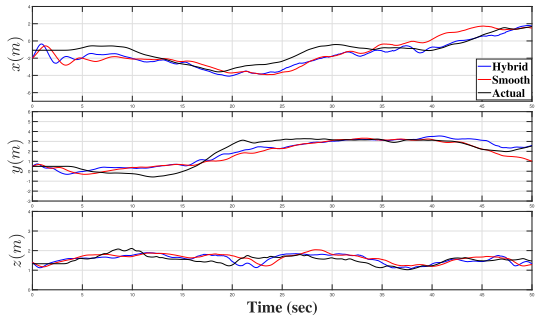

FIGURE 7. True position and estimated positions in the x, y and z direction.

TABLE 1. Comparison of the execution times by UKF, Right-UKF-LG, and the proposed observer.

Filters	Time (sec)
Conventional UKF	30
Right-UKF-LG	32
Proposed observer	22

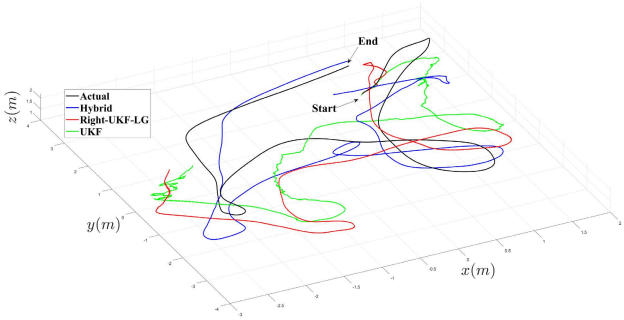

FIGURE 8. Comparison of global trajectories estimated by proposed observer, UKF, and Right-UKF-LG on V1_02_medium sequence.

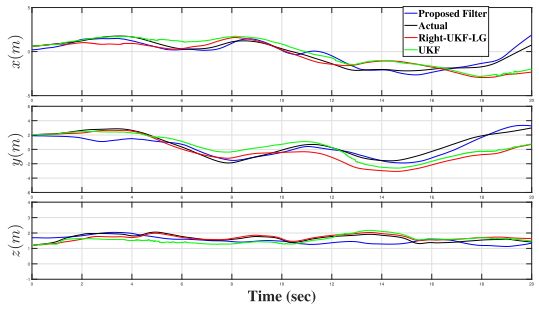

FIGURE 9. Actual position and estimated positions in the x, y and z direction.

initialized with the true values while the proposed observer is randomly initialized. It can be ascertained from these figures that, despite the random initialization for the proposed observer, it features superior performance when compared with the UKF and Right-UKF-LG on both trajectory tracking and reducing the effect of noise. Moreover, Table 1 summarizes the execution times of the three algorithms. It can be deduced from Table 1 that the hybrid observer is capable

of obtaining superior performance with less computational time compared with the UKF and Right-UKF-LG. Moreover, Table 1 also indicates that the proposed observer is more suitable for real-time implementation.

V. CONCLUSION

The present paper has investigated the problem of global convergence in SLAM observers. State-of-the-art SLAM techniques can only guarantee almost global convergence because of the non-contractibility of the state-space of attitude. Accordingly, the present paper has introduced a gradient-based hybrid observer to overcome topological obstructions and achieve global convergence. The proposed algorithm was demonstrated to be globally asymptotically convergent. Additionally, a new projection mechanism was introduced to tackle integral action for preserving the estimated bias in a predefined bound. Experimental and simulation results were provided to demonstrate the key advantages of the proposed algorithm.

SOME USEFUL IDENTITIES

The current paper uses the following identities related to the orthogonal projection and matrix inner product.

$$\Upsilon(\mathcal{X}B) = \Upsilon(\mathcal{X}^{-T}B), \quad (a)$$

$$\langle \mathcal{V}, B\rangle = \langle \mathcal{V}, \Upsilon(B)\rangle = \langle \Upsilon(B), \mathcal{V}\rangle, \quad (b)$$

$$\mathrm{tr}(ABCD) = \mathrm{tr}(CDAB) = \mathrm{tr}(DABC), \quad (c)$$

$$|\mathrm{tr}(AB)| \leq \sum_{i=1}^{n} \sigma_i(A)\sigma_i(B), \quad (d)$$

$$\mathrm{tr}(\mathcal{X}^T\mathcal{X}\Upsilon(B)\Upsilon(B)^T) = \mathrm{tr}(\Upsilon(B)\Upsilon(B)^T), \quad (e)$$

REFERENCES

[1] J. M. Aitken, M. H. Evans, R. Worley, S. Edwards, R. Zhang, T. Dodd, L. Mihaylova, and S. R. Anderson, "Simultaneous localization and mapping for inspection robots in water and sewer pipe networks: A review," *IEEE Access*, vol. 9, pp. 140173–140198, 2021.

[2] T. Bailey and H. Durrant-Whyte, "Simultaneous localization and mapping (SLAM): Part II," *IEEE Robot. Autom. Mag.*, vol. 13, no. 3, pp. 108–117, Sep. 2006.

[3] H. Bavle, P. De La Puente, J. P. How, and P. Campoy, "VPS-SLAM: Visual planar semantic SLAM for aerial robotic systems," *IEEE Access*, vol. 8, pp. 60704–60718, 2020.

[4] R. Mahony and T. Hamel, "A geometric nonlinear observer for simultaneous localisation and mapping," in *Proc. IEEE 56th Annu. Conf. Decis. Control (CDC)*, Dec. 2017, pp. 2408–2415.

[5] R. Mur-Artal, J. M. M. Montiel, and J. D. Tardós, "ORB-SLAM: A versatile and accurate monocular SLAM system," *IEEE Trans. Robot.*, vol. 31, no. 5, pp. 1147–1163, Oct. 2015.

[6] J. Luo and H.-L. Ko, "UKF-based inverted ultra-short baseline SLAM with current compensation," *IEEE Access*, vol. 10, pp. 67329–67337, 2022.

[7] S. Hashemi and A. Alfi, "Doppler and bearing tracking using fuzzy adaptive unscented Kalman filter," *Iranian J. Fuzzy Syst.*, vol. 16, no. 4, pp. 97–114, 2019.

[8] S. H. Hashemi, A. Alfi, S. University, and S. University, "Doppler and bearing tracking using adaptive modified covariance extended Kalman filter," *J. Control*, vol. 12, no. 4, pp. 23–33, Mar. 2019.

[9] S. H. Hashemi and N. Pariz, "Adaptive transformed unscented simplex cubature Kalman filter for target tracking," *IETE J. Res.*, vol. 2021, pp. 1–9, May 2021, doi: 10.1080/03772063.2021.1919223.

[10] Y. Song, Z. Zhang, J. Wu, Y. Wang, L. Zhao, and S. Huang, "A right invariant extended Kalman filter for object based SLAM," *IEEE Robot. Autom. Lett.*, vol. 7, no. 2, pp. 1316–1323, Apr. 2021.

[11] M. Tang, Z. Chen, and F. Yin, "Robot tracking in SLAM with Masreliez-Martin unscented Kalman filter," *Int. J. Control, Autom. Syst.*, vol. 18, no. 9, pp. 2315–2325, Sep. 2020.

[12] G. P. Huang, A. I. Mourikis, and S. I. Roumeliotis, "Analysis and improvement of the consistency of extended Kalman filter based SLAM," in *Proc. IEEE Int. Conf. Robot. Autom.*, May 2008, pp. 473–479.

[13] H. He, K. Wang, and L. Sun, "A SLAM algorithm of fused EKF and particle filter," in *Proc. WRC Symp. Adv. Robot. Autom. (WRC SARA)*, Aug. 2018, pp. 172–177.

[14] M. S. Bahraini, "On the efficiency of SLAM using adaptive unscented Kalman filter," *Iranian J. Sci. Technol., Trans. Mech. Eng.*, vol. 44, no. 3, pp. 727–735, Sep. 2020.

[15] R. Havangi, "Robust slam: Slam base on H_∞ square root unscented Kalman filter," *Nonlinear Dyn.*, vol. 83, no. 1, pp. 767–779, 2016.

[16] D. E. Zlotnik and J. R. Forbes, "Gradient-based observer for simultaneous localization and mapping," *IEEE Trans. Autom. Control*, vol. 63, no. 12, pp. 4338–4344, Dec. 2018.

[17] M. Wang and A. Tayebi, "Geometric nonlinear observer design for SLAM on a matrix lie group," in *Proc. IEEE Conf. Decis. Control (CDC)*, Dec. 2018, pp. 1488–1493.

[18] H. A. Hashim and A. E. E. Eltoukhy, "Landmark and IMU data fusion: Systematic convergence geometric nonlinear observer for SLAM and velocity bias," *IEEE Trans. Intell. Transp. Syst.*, vol. 23, no. 4, pp. 3292–3301, Apr. 2020.

[19] H. A. Hashim, "Guaranteed performance nonlinear observer for simultaneous localization and mapping," *IEEE Control Syst. Lett.*, vol. 5, no. 1, pp. 91–96, Jan. 2020.

[20] R. Mahony, T. Hamel, and J. Trumpf, "An homogeneous space geometry for simultaneous localisation and mapping," *Annu. Rev. Control*, vol. 51, pp. 254–267, 2021.

[21] P. van Goor, R. Mahony, T. Hamel, and J. Trumpf, "A geometric observer design for visual localisation and mapping," in *Proc. IEEE 58th Conf. Decis. Control (CDC)*, Dec. 2019, pp. 2543–2549.

[22] P. V. Goor, R. Mahony, T. Hamel, and J. Trumpf, "An observer design for visual simultaneous localisation and mapping with output equivariance," *IFAC-PapersOnLine*, vol. 53, no. 2, pp. 9560–9565, 2020.

[23] P. van Goor, R. Mahony, T. Hamel, and J. Trumpf, "Constructive observer design for visual simultaneous localisation and mapping," *Automatica*, vol. 132, Oct. 2021, Art. no. 109803.

[24] P. Mäkinen, M. M. Aref, J. Mattila, and S. Launis, "Application of simultaneous localization and mapping for large-scale manipulators in unknown environments," in *Proc. IEEE Int. Conf. Cybern. Intell. Syst. (CIS) IEEE Conf. Robot., Automat. Mechatronics (RAM)*, Nov. 2019, pp. 559–564.

[25] M. Wang and A. Tayebi, "Hybrid pose and velocity-bias estimation on SE(3) using inertial and landmark measurements," *IEEE Trans. Autom. Control*, vol. 64, no. 8, pp. 3399–3406, Aug. 2018.

[26] S. H. Hashemi, N. Pariz, and S. K. H. Sani, "Observer-based adaptive hybrid feedback for robust global attitude stabilization of a rigid body," *IEEE Trans. Aerosp. Electron. Syst.*, vol. 57, no. 3, pp. 1919–1929, Jun. 2021.

[27] S. H. Hashemi, N. Pariz, and S. K. Hosseini Sani, "Observer-based hybrid control for global attitude tracking on SO(3) with input quantisation," *Int. J. Control*, vol. 2022, pp. 1–12, Feb. 2022, doi: 10.1080/00207179.2022.2043564.

[28] M. Wang and A. Tayebi, "Globally asymptotically stable hybrid observers design on SE (3)," in *Proc. IEEE 56th Annu. Conf. Decis. Control (CDC)*, Dec. 2017, pp. 3033–3038.

[29] M. Wang and A. Tayebi, "A globally exponentially stable nonlinear hybrid observer for 3D inertial navigation," in *Proc. IEEE Conf. Decis. Control (CDC)*, Dec. 2018, pp. 1367–1372.

[30] M. Wang and A. Tayebi, "Hybrid nonlinear observers for inertial navigation using landmark measurements," *IEEE Trans. Autom. Control*, vol. 65, no. 12, pp. 5173–5188, Dec. 2020.

[31] M. Wang and A. Tayebi, "Nonlinear state estimation for inertial navigation systems with intermittent measurements," *Automatica*, vol. 122, Dec. 2020, Art. no. 109244.

[32] R. Goebel, R. G. Sanfelice, and A. Teel, "Hybrid dynamical systems," *IEEE Control Syst. Mag.*, vol. 29, no. 2, pp. 28–93, Apr. 2009.

[33] A. R. Teel, F. Forni, and L. Zaccarian, "Lyapunov-based sufficient conditions for exponential stability in hybrid systems," *IEEE Trans. Autom. Control*, vol. 58, no. 6, pp. 1591–1596, Jun. 2012.

[34] S. H. Hashemi, N. Pariz, and S. K. Hosseini Sani, "Global exponential stabilization of a quadrotor by hybrid control," *Trans. Inst. Meas. Control*, vol. 43, no. 10, pp. 2345–2357, Jun. 2021.

[35] J.-C. Bourin, "Matrix versions of some classical inequalities," *Linear Algebra its Appl.*, vol. 416, nos. 2–3, pp. 890–907, Jul. 2006.
[36] R. Moghe and M. Akella, "Projection scheme and adaptive control for symmetric matrices with eigenvalue bounds," *IEEE Trans. Autom. Control*, early access, Feb. 23, 2022, doi: 10.1109/TAC.2022.3153458.
[37] L. Mirsky, "A trace inequality of John von Neumann," *Monatshefte fur-Math.*, vol. 79, no. 4, pp. 303–306, 1975.
[38] M. Brossard, S. Bonnabel, and A. Barrau, "Invariant Kalman filtering for visual inertial SLAM," in *Proc. 21st Int. Conf. Inf. Fusion (FUSION)*, Jul. 2018, pp. 2021–2028.
[39] M. Burri, J. Nikolic, P. Gohl, T. Schneider, J. Rehder, S. Omari, M. W. Achtelik, and R. Siegwart, "The euroc micro aerial vehicle datasets," *Int. J. Robot. Res.*, vol. 35, no. 10, pp. 1157–1163, 2016.
[40] S. Umeyama, "Least-squares estimation of transformation parameters between two point patterns," *IEEE Trans. Pattern Anal. Mach. Intell.*, vol. 13, no. 4, pp. 376–380, Apr. 1991.

SEYED HAMED HASHEMI received the B.Sc. degree in electrical engineering from the Babol Noshirvani University of Technology (BNUT), Iran, in 2014, the M.Sc. degree in electrical engineering-control from the Shahrood University of Technology (SUT), Iran, in 2017, and the Ph.D. degree in electrical engineering-control from the Ferdowsi University of Mashhad (FUM), Iran, in 2021. He is currently a Postdoctoral Research Fellow with the Faculty of Engineering and aturalaturalN Sciences, Unit of Automation Technology and Mechanical Engineering, Tampere University. His research interests include topological constraints in control systems, the control of hybrid systems, simultaneous localization and mapping (SLAM), and estimation theory.

JOUNI MATTILA received the M.Sc. and Ph.D. degrees in automation engineering from the Tampere University of Technology, Tampere, Finland, in 1995 and 2000, respectively. He is currently a Professor of machine automation with the Unit of Automation Technology and Mechanical Engineering, Tampere University. His research interests include machine automation, nonlinear model-based control of robotic manipulators, and energy-efficient control of heavy-duty mobile manipulators.